

Functionalization of Cobalt Ferrite Nanoparticles by a Vitamin C-assisted Covering with Gold

Regular Paper

Arūnas Jagminas^{1,*}, Kęstutis Mažeika¹, Rokas Kondrotas¹,
Marija Kurtinaitienė¹, Aldona Jagminiene¹ and Agnė Mikalauskaitė¹

¹ State Research Institute Center for Physical Sciences and Technology, Vilnius, Lithuania

* Corresponding author E-mail: jagmin@ktl.mii.lt

Received 28 Oct 2013; Accepted 6 Mar 2014

DOI: 10.5772/58453

© 2014 The Author(s). Licensee InTech. This is an open access article distributed under the terms of the Creative Commons Attribution License (<http://creativecommons.org/licenses/by/3.0>), which permits unrestricted use, distribution, and reproduction in any medium, provided the original work is properly cited.

Abstract We report the design and methodology for functionalization of the surface of small Co-ferrite nanoparticles with a mean size of up to 5.0 nm through the attachment of vitamin C molecules initiating $[\text{AuCl}_4]$ reduction and the subsequent deposition of gold. By this method, Co-ferrite-Au nanoparticles have been fabricated for the first time in a simple and controllable manner, consisting of the determination of the consumed ascorbic acid content. The sequential addition of vitamin C and HAuCl_4 to the ferrofluid at low concentrations leads to the formation of a gold shell on the ferrite core. This approach avoids the additional stabilization of ferrite nanoparticles before gold deposition, and is of great importance in view of the preparation of biodegradable superparamagnetic particles for nanomedicine applications.

The deposition of gold onto the ferrite surface was proved herein by UV-vis absorption and energy-dispersive X-ray (EDX) spectroscopy, inductively coupled plasma mass spectrometry analysis, atomic force microscopy (AFM), high resolution transmission electron microscopy (HRTEM) and Mössbauer spectroscopy.

Keywords Magnetic Nanoparticles, Co-ferrite, Gold Deposition, Characterization

1. Introduction

In recent years, the application of magnetic nanoparticles (NPs) in gene therapy, target drug delivery, biological sensing, biomolecule separation and magnetic resonance imaging, has received a great deal of attention [1-8]. For the subsequent attachment of specific biomarkers to the surface of superparamagnetic iron oxide NPs, it is necessary to either coat them with a thin gold shell or else decorate them with small gold seeds in a cost-efficient and reproducible way. Besides, the coating of the surface of magnetic NPs with a gold shell is essential in seeking to improve NPs biocompatibility and the chemical resistance of magnetic cores [9,10]. Based on this requirement, several methods, such as sonochemical treatment, galvanic replacement, reverse micelles, laser ablation and chemical reduction, among others, have been reported over the past decade for the attachment of

gold to the surface of magnetite (Fe_3O_4) and maghemite ($\gamma\text{-Fe}_2\text{O}_3$) NPs [11-21]. For example, Lin et al. [11] have synthesized core/shell Fe/Au NPs by a reverse-micelle approach. Hierarchical dumbbell-like Au- Fe_3O_4 NPs have been synthesized via the decomposition of $\text{Fe}(\text{CO})_5$ on the surface of Au NPs [22]. Magnetite/maghemite NPs, with an average size of ~60 nm, have been coated with a gold shell by the reduction of Au(III) ions via iterative hydroxylamine seeding [13]. A complete covering of magnetite NPs by gold has also been realized through the attachment of gold seeds together with amino-modified silica particles, stabilized with oleic and 2-bromo-2-propionic acids, and the subsequent formation of a gold shell with the seeds' enlargement upon a prolonged reduction of gold ions [14]. Similar strategies have also been reported for fabrication of Fe_3O_4 -organosilane-Au and Co-organosilane-Au NPs [14,15]. In this way, the initial size of Fe_3O_4 NPs (~10 nm) and Co NPs (~12 nm) increased up to 100 nm and more and became too large for application in magnetic resonance imaging [23]. Several protocols have also been reported for the direct covering of iron oxide NPs by the reduction of Au(III) species with NH_4OH [24-28]. In fact, all these methods have been devoted to the covering or decoration of $\gamma\text{-Fe}_2\text{O}_3$ NPs because the formation of a gold shell on a magnetite (Fe_3O_4) surface by a common approach involving citrate or the borohydride reduction of auric salts is problematic; in most cases, the reduction resulted in the formation of pure gold species [12,16]. Moreover, to explore the magnetization of core/shelled NPs for magnetic separation or imagining together with gold-protein binding reactivity and biocompatibility, the thickness and uniformity of the gold shell should be controlled simply and precisely during the fabrication. Besides, the magnetic core could not be consumed for the reduction of Au(III) species or dissolved during plating [29].

To satisfy all these requirements, we describe in this article a new process for the direct covering of small ($\text{O}_{\text{mean}} = 2.0 - 5.0$ nm) Co-ferrite NPs with gold in which as-grown by co-precipitation way CoFe_2O_4 NPs are stabilized with vitamin C (VitC), later behaving as surface-initiated reducers of $[\text{AuCl}_4^-]$ ions. We note that this method differs from others reported to date for the direct coating of magnetic NPs by a gold shell as regards such aspects as the core material's nature (CoFe_2O_4), small NPs (mean size ≤ 5 nm), a biodegradable reductant (VitC) and a simply-controllable processing regime. To the best of the author's knowledge, the covering of superparamagnetic cobalt ferrite NPs by gold seeds or a shell has not yet been reported. We note, however, that these NPs have been used in tests carried out together with scientists from the Institute of Oncology at Vilnius University in targeting human pancreatic and ovarian cancer cells. These results will be presented in a separate paper. It is also expected that the tethering of Au^0 species

to the surface of larger CoFe_2O_4 NPs with $\text{O}_{\text{mean}} = 15\text{-}20\text{nm}$ can be synthesized, as reported recently in [30], and should also be valid according to the manner proposed in this study.

2. Experimental

2.1 Chemicals

All the reagents used in this study were of at least analytical grade and, except for NaOH, used without any further purification. The CoCl_2 , $\text{Fe}_2(\text{SO}_4)_3$, HAuCl_4 and citric acid were purchased from Aldrich Chemicals Inc. The ascorbic acid was obtained from Rechem Slovakia and the NaOH was purchased from Poch SA (Poland) and purified by the preparation of a saturate solution resulting in the crystallization of other sodium salts. Deionized distilled water was used throughout all the experiments.

2.2 Synthesis of Co-ferrite NPs

In this study, Co-ferrite NPs were synthesized from the complex-assisted alkaline solutions of Co(II) and Fe(III) salts in a thermostated glass reactor by the co-precipitation method at 80 °C and ambient pressure for 3 h. The working solution was prepared from CoCl_2 and $\text{Fe}_2(\text{SO}_4)_3$ salts and 100 mmol/L citric acid; the total metal salt concentration was 100 mmol/L. In order to obtain the stoichiometric composition of the NPs, the initial mole concentration of the CoCl_2 and $\text{Fe}_2(\text{SO}_4)_3$ precursors in the reaction medium was set at 1.1:1 [30]. All the solutions were deoxygenated with argon before mixing. The pH of the solutions was kept at a level of 12.1 by the addition of a 5.0 mol/L NaOH solution. The required quantity of the NaOH solution in each case was determined by an additional blank experiment. In the subsequent experiment, this quantity was placed in the reactor and mixed with the other components, with several seconds of vigorous stirring. The synthesis in the thermostated reactor was carried out under a continuous argon gas bubbling. The as-grown products were centrifuged at 8,500 rpm for 3 min. and carefully rinsed five times using new portions (10 mL) of H_2O . The supernatants of the last three centrifugations were combined and neutralized by the addition of ascorbic acid or vitamin C 0.05 mol/L solutions to a pH range of 6.0 to 5.5. The ferrofluid obtained and the collected NPs were studied and subjected to further processing over the following week.

2.3 Gold Shell Formation

The surface-initiated deposition of the gold shell onto the Co-ferrite surface was investigated via the stabilization of as-grown NPs by VitC or ascorbate ions' attachment instead of OH^- and the subsequent addition of a HAuCl_4 solution in low concentration. The thickening of the gold

shell was attained via the further addition of *VitC* and $[\text{AuCl}_4^-]$ species in low concentration doses at ambient temperature. The products obtained were collected and examined by TEM, EDX and UV-vis spectrophotometry.

2.4 Analysis

The concentration of *NPs* (N_i) was calculated after the estimation of the total amount of CoFe_2O_4 in the ferrofluid (m_n) and the average size and weight of individual *NPs* (m_i):

$$N_i = m_n / m_i \quad (1)$$

In the calculations, the density of the CoFe_2O_4 was considered to be 5.29 g cm^{-3} . The total amount of CoFe_2O_4 as well as the stoichiometry of the *NPs*' material were estimated via the determination of the cobalt and iron contents after the *NPs*' dissolution in a HCl (1:1) solution by inductively-coupled plasma mass spectrometry. Measurements were made on emission peaks at 228.616 nm and 239.562 nm for the Co and Fe, respectively, using an OPTIMA 7000DV (Perkin Elmer, USA) spectrometer. Calibration curves were made from dissolved standards within 1 to 50 ppm concentrations in the same acid matrix as the unknowns. The standards and unknowns were analysed at least four times. The detection limits based on three standard deviations resulted in a $\pm 2.6 \%$ error.

2.5 Characterization

The morphology of the as-grown products was investigated using a transmission electron microscope (TEM, model MORGAGNI 268) operated at an accelerating voltage of 72 keV. The *NPs* subjected to TEM observations were dispersed in ethanol and drop-cast onto the carbon-coated copper grid. The average size of the *NPs* was estimated from at least 200 species observed in their TEM images. HRTEM studies of the as-synthesized products were performed using a LIBRA 200 FE at an accelerating voltage of 200 keV. The morphology of ultra-small Co ferrite *NPs*, spin-coated onto the mica substrate, was investigated with an atomic force microscope Veeco AFM diInnova in a tapping mode.

X-ray powder diffraction experiments were performed on a D8 diffractometer (Bruker AXS, Germany), equipped with a Göbel mirror as a primary beam monochromator for $\text{CuK}\alpha$ radiation. Mössbauer spectra were collected in the transmission geometry from the spot of the synthesized *NPs* formed on a shred of filter paper using a $\text{Co}^{57}(\text{Rh})$ source. A closed-cycle He cryostat (Advanced Research Systems, Inc.) was used for low temperature measurements. The hyperfine field B distributions and separate sextets or doublets were applied to fit the experimental spectra and determine the average hyperfine field $\langle B \rangle$ using the WinNormos (Site, Dist) software. The transition temperature from a superparamagnetic to a

magnetic state was determined at a temperature when $\langle B \rangle \approx 0.5B_0$, where B_0 is the maximum hyperfine field observed at the lowest temperature.

3. Results and discussion

3.1 Fabrication and characterization of Co-ferrite *NPs*

In this study, small ($1.6 \leq \varnothing_{\text{mean}} \leq 5.0 \text{ nm}$) cobalt ferrite, CoFe_2O_4 , *NPs*, prospective for magnetic resonance imaging [31], were synthesized by a citric acid-assisted co-precipitation reaction of Co(II) and Fe(III) species in the degassed alkaline (pH 12.1) solution at $80 \text{ }^\circ\text{C}$ for 3 h followed by several rinsing and centrifugation procedures. With TEM and AFM, the resulting Co-ferrite *NPs* remained in the supernatant after washings and centrifugations at 8,500 rpm for 3 min. and were fairly spherical $1.6 \pm 1.0 \text{ nm}$ in diameter (Figure 1). The analysis of the TEM images of the Co ferrite *NPs* separated from the ultra-small ones by centrifugation revealed their narrow size dispersion between 4.0 and 6.0 nm (Figure 2). EDX and chemical analysis of *NPs* dissolved in a HCl solution (1:1) by inductively-coupled plasma mass spectrometry indicated the same CoFe_2O_4 stoichiometric composition. The crystalline nature of cobalt ferrite *NPs* was also characterized by X-ray diffraction. The representative XRD pattern of these *NPs* is shown in Figure 2b. It should be emphasized that the positions and relative intensities of all the diffraction peaks match well with standard CoFe_2O_4 diffraction data, implying the *NPs* polycrystalline inverse spinel structure.

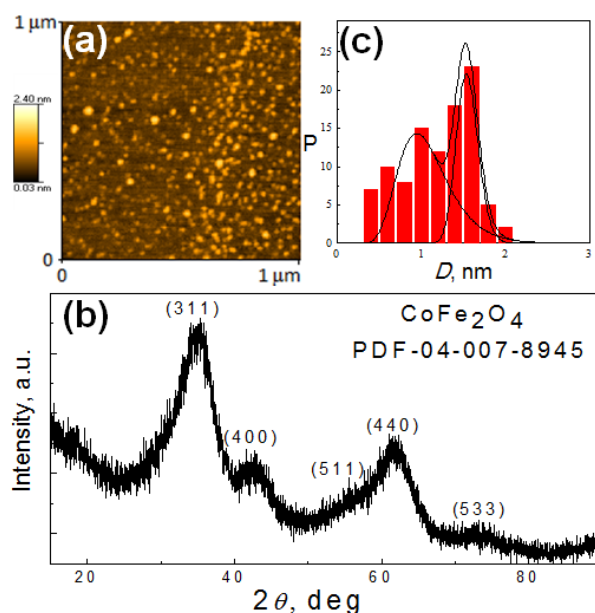


Figure 1. AFM (a) image and XRD pattern (b) of ultra-small Co-ferrite *NPs* synthesized by a co-precipitation reaction from an alkaline (pH=12.1) de-aerated solution containing 100 mmol/L $\text{CoCl}_2 + \text{Fe}_2(\text{SO}_4)_3$ at a 1.1:1.0 ratio + 100 mmol/L citric acid at $80 \text{ }^\circ\text{C}$ for 3 h (supernatant fraction). In (c), the histogram and lognormal (lines) distribution of the *NPs*' sizes are shown.

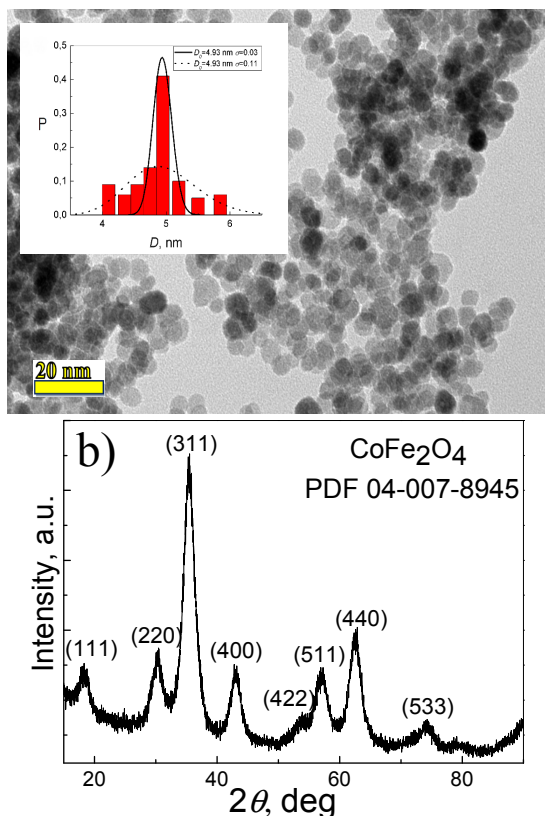


Figure 2. A TEM (a) view of CoFe_2O_4 NPs synthesized as in Figure 1 and collected by centrifugation at 8,500 rpm for 3 min. In (b), a typical XRD pattern of the as-grown product is shown. Inset: histogram and lognormal (line) distribution of the NPs' sizes.

3.2 Strategy for controllable Co-ferrite-Au fabrication

The strategy for covering Co-ferrite NPs by gold in an aqueous solution was based on the use of a *VitC* attachment to the NPs' surface and a subsequent reduction of $[\text{AuCl}_4]^-$ ions under sonication at room temperature. In general, both the *VitC* and ascorbic acid in aqueous solutions possess an intense and sensitive absorption band in a vicinity of 263 nm, whose intensity increases linearly with acid concentration from 0 to 40 $\mu\text{mol/L}$ (Figure 3). We suspected that this property should allow for controlling the quantity of the reduced gold through the reaction:



Furthermore, we found that the neutralization of Co-ferrite ferrofluids to a stable pH value within a 6.0-5.5 pH range by the addition of ascorbic acid or *VitC* at room temperature is a time-consuming process involving intense stirring for 30 min. or longer - probably due to the slow replacement of the attached OH^- ions by the ascorbate ones. Therefore, various *VitC* attachment levels can be organized for as-grown magnetic NPs by controlling the time for neutralization and the content of the ascorbic acid or *VitC* consumed. Note that the high

stability of ultra-small Co-ferrite NPs fabricated by coprecipitation under the conditions of this study remained approximately the same after neutralization with *VitC* or ascorbate ions.

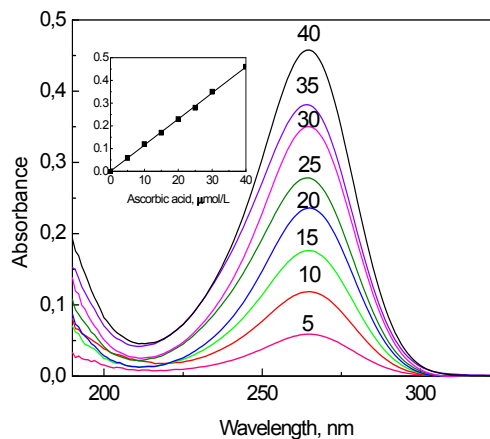


Figure 3. Absorbance spectra for different concentrations of ascorbic acid from 5 to 40 $\mu\text{mol/L}$. Inset: calibration plot of ascorbic acid at $\lambda = 263$ nm.

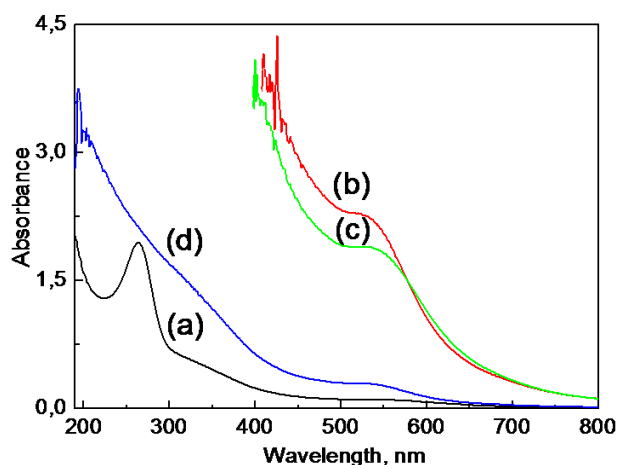


Figure 4. Absorption spectra of ultra-small Co-ferrite NPs grown as in Figure 1 and neutralized by ascorbic acid to $\text{pH} = 6.0$ (a) at various stages of their subsequent sonication with 0.4 mmol/L HAuCl_4 at ambient temperature for one (b), two (c) and three (d) days. After the first and second days, 0.15 mL of ascorbic acid (0.05 mol/L) and 0.4 mL of HAuCl_4 (0.01 mol/L) were added for further gold reduction. For spectra (a) and (d), the ferrofluids were diluted 16 times whereas the contributions of spectra (b) and (c) in the UV region are not shown due to the strong oscillations typical of concentrated solutions.

According to the UV-vis spectra, presented in Figure 4 - the addition of just 0.4 mmol/L $[\text{AuCl}_4]^-$ species into neutralized Co-ferrite NPs' ferrofluid at ambient temperature results in a decrease in the number of ascorbate ions. The prolonged sonication of *VitC*-modified Co-ferrite NPs in a solution containing $[\text{AuCl}_4]^-$ (even at room temperature) leads to a decrease in the amount of adsorbed ascorbate ions down to zero (curve d). With the further addition of *VitC* and Au(III) species, the

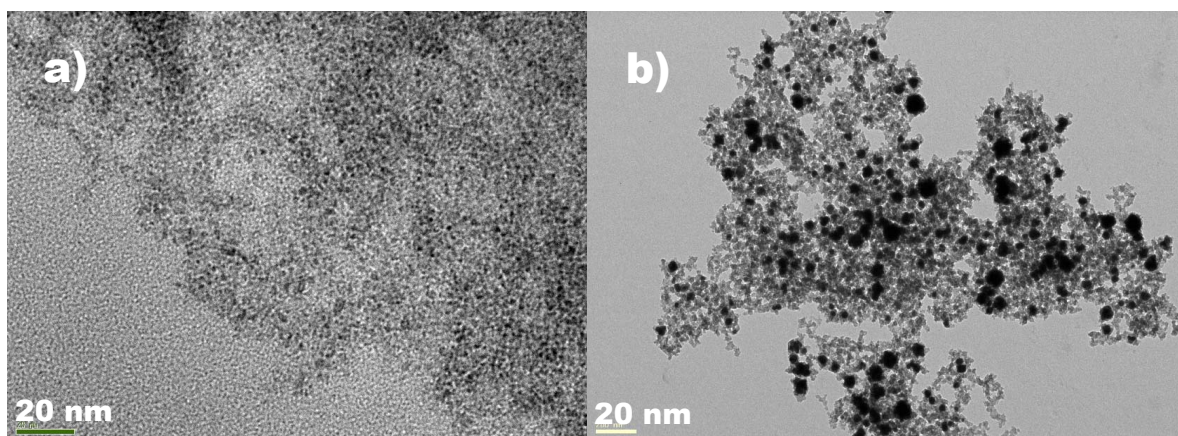


Figure 5. A TEM view of Co-ferrite NPs, fabricated as in Figure 1 after the neutralization of a 10 mL suspension from pH 10.2 to pH 6.0 with ascorbic acid under ultrasonic agitation for 10 min, a subsequent addition of 0.4 mL HAuCl₄ (10 mmol/L) and sonication for 24 h at room temperature with initial 20 μmol (a) or 60 μmol (b) ascorbic acid content.

colour of the ferrofluid changes to violet and pinkish tints as seen by a naked eye. The corresponding UV-vis spectra for these ferrofluids are also shown in Figure 4 (curves b and c), indicating that the appearance and variation within a wide plasmonic absorption band peaked in the vicinity of 520-540 nm, characteristic of nm-scaled gold crystals [32]. With an increase in the chemical precipitation time, this absorption band red-shifts towards longer wavelengths and lower energies, signalling the increase in the size of the gold species [33].

3.3 TEM and HRTEM observations

Figure 5 depicts a set of TEM micrographs of Co-ferrite ferrofluid NPs obtained after 24 h of [AuCl₄]⁻ ions' reduction with ascorbic acid molecules consumed for the neutralization of NPs to pH 6.0 (image a) and the further addition of HAuCl₄ (image b). From image (a), any obvious changes can be viewed in the morphology of ultra-small Co-ferrite NPs after the consumption of ascorbic acid used only for their neutralization. However, the subsequent addition of ascorbic acid and HAuCl₄ results in the appearance and growth of separate Au⁰ nm-scaled crystals (image b). In contrast, we have observed that the functionalization of ultra-small Co-ferrite NPs with VitC (instead of ascorbic acid) results in a higher TEM images contrast after their incubation with [AuCl₄]⁻ ions just after one day (Figures 6a and b). Moreover, from the TEM observations, the formation of separate gold crystals in a ferrofluid bulk was not detected when Co-ferrite NPs were neutralized with VitC. With further addition of VitC and [AuCl₄]⁻ ions, separate crystals of pure gold were also not formed under ambient conditions. However, the evidence of gold deposition can be inferred from an EDX spectrum (Figure 6c), in which iron, cobalt, oxygen, copper (from TEM grid) and gold elements were detected in the scope of the NPs.

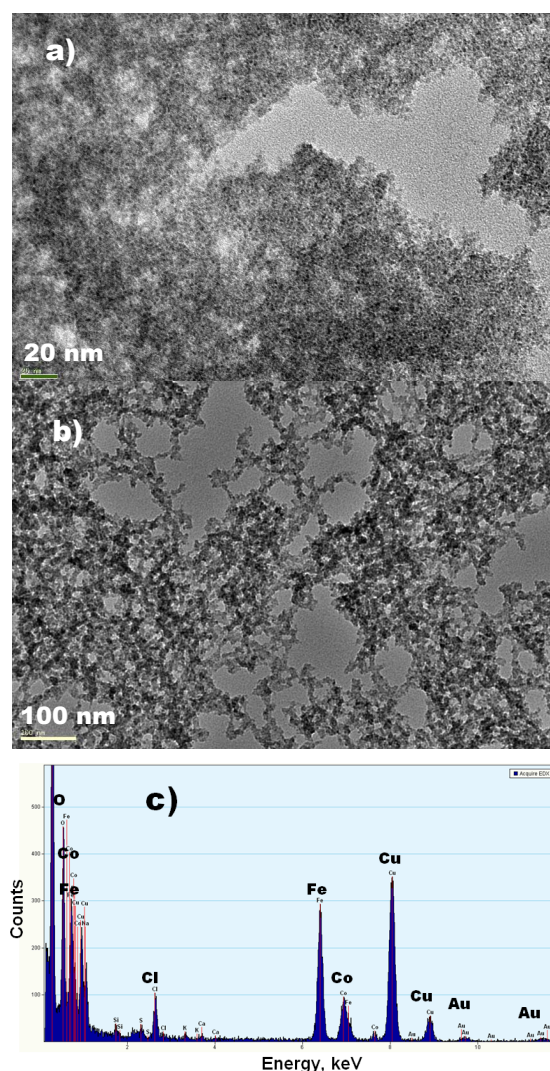


Figure 6. TEM views of Co-ferrite NPs, fabricated as in Figure 1 after the neutralization of a 10 mL suspension from pH 10.2 to pH 6.0 with VitC under ultrasound agitation for 10 min and (a) a subsequent sonication at room temperature for 12 h with 0.4 mL HAuCl₄ (10 mmol/L) and, after further sonication, with a new dose (0.2 mL) of VitC (50 mmol/L) for 5 h (b). In (c): EDX spectrum of the synthesized product.

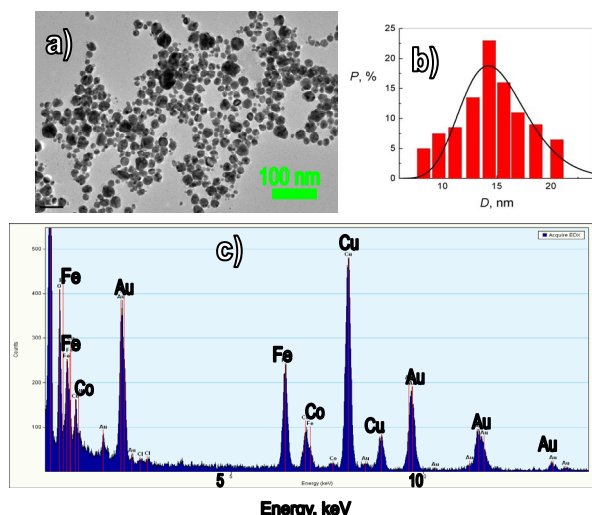


Figure 7. (a) TEM view of CoFe_2O_4 -Au NPs synthesized as in Figure 2 after surface functionalization with *VitC* and the reduction of $[\text{AuCl}_4]^-$ ions through two days' sonication in a 20 $\mu\text{mol/L}$ HAuCl_4 solution containing *VitC* in excess. (b) depicts the histogram and log-normal distribution of functionalized NPs, whereas the EDX spectrum of the obtained NPs is shown in (c).

Furthermore, in the case of larger Co-ferrite NPs with a mean size of ~ 5.0 nm, the increase in the $[\text{AuCl}_4]^-$ reduction time upon further additions of *VitC* and HAuCl_4 resulted in an increase in the NPs' mean size up to 15.0 nm (Figure 7), signalling the formation of CoFe_2O_4 doped with Au NPs and their size increase with processing time. Three portions of 10 mmol HAuCl_4 solution in the 0.3 mL doses were added to 20 mL of suspension containing ~ 10 mg/L CoFe_2O_4 NPs in order to give a pinkish colour to the suspension. From statistical analyses, the size distribution

of the CoFe_2O_4 -Au NPs is not broad (see Figure 7b). From high-resolution transmission electron micrographs of the CoFe_2O_4 -Au NPs with a final mean size of about 15 nm (Figure 7a) and obtained with a gold deposition approach using *VitC*, it was found that the lattice fringes taken from the surface of these NPs (initial size ~ 5.0 nm) after three days' sonication with *VitC* and $[\text{AuCl}_4]^-$ ions showed interplanar spacing of 2.01 Å and 2.35 Å, which corresponds to the fcc-structured gold (200) and (111) planes, respectively, indicating the formation of CoFe_2O_4 doped with Au.

3.4 Mössbauer spectroscopy for ultra-fine Co ferrite-Au NPs

The key questions that should be answered as regards the fabrication of prospective NPs for nanomedicine applications concern their size, size dispersity and the thickness of their shells. According to the literature [34], the covering of magnetite NPs with a gold shell results in a decrease in magnetization and the blocking temperature (T_B). Hence, to preserve the Fe oxide core's magnetism, the gold shell ought to be uniform and as thin as possible. In this study, the influence of the deposited gold on the magnetic properties of the Co-ferrite core material was ascertained from the T_B of NPs determined from the Mössbauer spectra variables with the recording temperature. In this setup, various dried NPs and their ferrofluid probes were initially cooled to ~ 10 K and the Mössbauer spectra were recorded in transmission mode. A set of Mössbauer spectra was further recorded as the temperature was increased. Note that T_B indicates the temperature above which NPs are superparamagnetic.

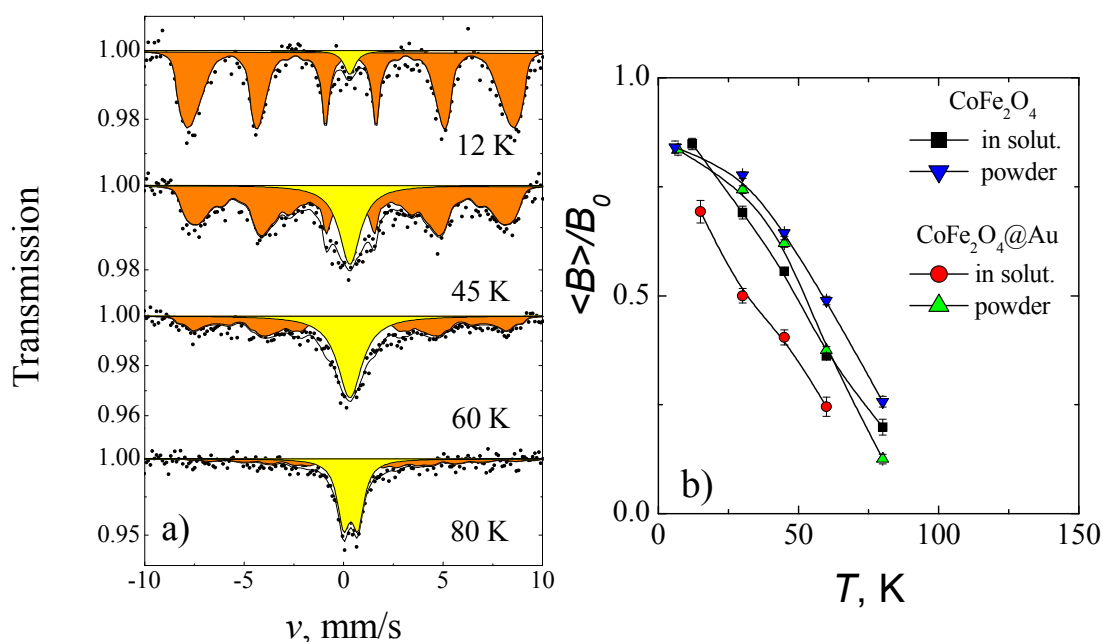


Figure 8. (a) Mössbauer spectra of CoFe_2O_4 NPs ($\varnothing_{\text{mean}} = 1.6$ nm) dispersed in an aqueous solution before Au deposition at indicated temperatures and (b) the dependences of a normalized average hyperfine field for the same CoFe_2O_4 NPs before and after Au deposition in the solution and powder state on temperature, as indicated

Typical Mössbauer spectra of pure Co-ferrite NPs with $\varnothing_{\text{mean}} = 1.6$ nm in the aqueous ferrofluid at various recording temperatures are depicted in Figure 8a, while the variations in the calculated hyperfine fields for the gold-covered NPs with temperature are presented in Figure 8b. As seen, the NPs covered with gold in dry and ferrofluid states demonstrate a somewhat lower T_B ; most likely this is due to the less-effective coupling of the magnetic dipole moments in larger CoFe_2O_4 -Au NPs.

4. Discussion

In this study, several crucial points for the deposition of a gold in a controllable manner were identified and can be discussed: (i) First of all, the application of *VitC* for the neutralization of as-grown magnetic NPs down to pH 6.0-7.0 is required. This procedure results in the binding of *VitC* molecules to the NPs' surfaces *via* the substitution of OH^- ions by ascorbate ions. The replacement of OH^- ions by ascorbate ions can be inferred from a further increase in the pH of the Co-ferrite NPs' medium, neutralized to pH 6.0, by ~ 0.2 pH/min during stirring for up to 0.5 h. (ii) We suspect that by being attached to the NPs' surfaces, the *VitC* molecules can initiate deposition and - as a weak reducing agent - reduce the $[\text{AuCl}_4]^-$ ions quite slowly under the mild reaction conditions, as shown by the scheme in Figure 9. After the subsequent addition of *VitC* and low concentration doses of Au(III) ions, the content of deposited gold can be simply controlled via the determination of the consumed content of the ascorbic acid by reaction (2). The excess of attached *VitC* ions results in the reduction of all the $[\text{AuCl}_4]^-$ species and the suppression of the reaction. In the case of a low *VitC* content attached to the NPs' surfaces, this effect can be simply proved by the disappearance of an absorption peak in the vicinity of 263 cm^{-1} in the corresponding UV-vis spectrum (Figure 4d). The amount of attached gold can also be seen from the changes in the NPs' suspension colour from black to violet and dark pink, seen both by the naked eye and by the occurrence of, and increase in the sedimentation of, CoFe_2O_4 -Au NPs with deposition time. (iii) Besides serving as a reducing agent, *VitC*, due to its strong adsorption affinity to the alkaline ferrite surface, is a ligand, protecting Co-ferrite NPs from aggregation. As a result of this effect, the stability of as-grown CoFe_2O_4 NPs after neutralization (even down to pH 5.5) was found to be at the same good level as stabilized by OH^- ions at pH 10.2-10.3. (iv) A sharp absorption peak of ascorbic acid as a main component of *VitC* in the vicinity of 263 cm^{-1} is key, allowing us to more easily control the deposition of gold onto the Co-ferrite NP surface, starting from the initial stages. The prevention of nucleation and the further growth of separate gold nanocrystals in the case of *VitC* usage will be analysed in a separate paper.

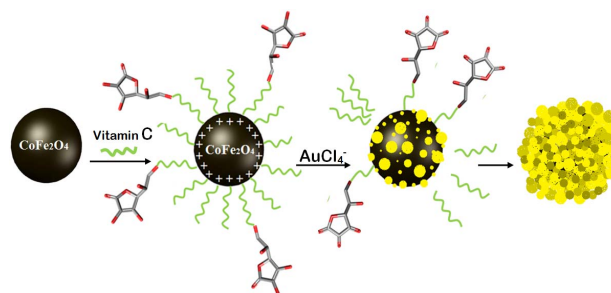


Figure 9. Schematic diagram illustrating the gold deposition process onto the surface of cobalt ferrite NPs *via* stabilization with Vitamin C, and the subsequent reduction of gold acid species

5. Conclusions

We have developed a simple method for covering of magnetic cobalt ferrite NPs with gold using vitamin C as a perfect reducing agent capable of binding with iron oxide. This approach differs from others reported to date in such aspects as the core material nature (CoFe_2O_4), the extremely small NP size (≤ 5.0 nm), the application of a biocompatible reductant (vitamin C), and the possibility of controlling the content of the deposited gold by a simple determination of the quantity of the consumed ascorbic acid. The deposition protocol developed in this study is easily scalable and can be adapted to cover other ferrite and magnetite NPs - produced by co-precipitation, with a gold.

6. Acknowledgements

Support for this work from the Lithuania Science Council Foundation under Grant No. MIP-088/2011 is gratefully acknowledged.

7. References

- [1] Graham L, Ferreira HA, Freitas PP (2004) Magnetoresistive-based biosensors and biochips. Trends in biotechnology 22: 455 – 462.
- [2] Gupta AK, Gupta, M (2005) Synthesis and surface engineering of iron oxide nanoparticles for biomedical applications. Biomater. 26: 3995 – 4021.
- [3] Laurent S, Forge D, Port M, Roch A, Robic C, Elst LV, Muller, RN (2008) Magnetic Iron Oxide Nanoparticles: Synthesis, Stabilization, Vectorization, Physicochemical Characterizations, and Biological Applications. Chem. Rev. 108: 2064 – 2110.
- [4] Ruiz-Hernandez E, Baeza A, Vallet-Regi M (2011) Smart Drug Delivery through DNA/Magnetic Nanoparticle Gates. ACS Nano 5: 1259 – 1266.
- [5] Latrigue L, Wilhelm C, Servais J, Factor C, Dencausse A, Bacri J-C, Luciani N, Gazeau F (2012) Nanomagnetic Sensing of Blood Plasma Protein Interactions with Iron Oxide Nanoparticles: Impact on Macrophage Uptake. ACS Nano 6: 2665 – 2678.

- [6] Maeda Y, Yoshino T, Matsunaga T (2009) Novel nanocomposites consisting of in vivo-biotinylated bacterial magnetic particles and quantum dots for magnetic separation and fluorescent labelling of cancer cells. *J. Mater. Chem.* 19: 6361 – 6366.
- [7] Takahashi M, Yoshino T, Takeyama H, Matsunaga T (2009) Direct magnetic separation of immune cells from whole blood using bacterial magnetic particles displaying protein G. *Biotechnology Progress* 25: 219 – 226.
- [8] Banerjee SS, Chen DH (2008) Multifunctional pH-sensitive magnetic nanoparticles for simultaneous imaging, sensing and targeted intracellular anticancer drug delivery. *Nanotechnology* 19: 505104.
- [9] Bao J, Chen W, Liu TT, Zhu Y, Jin P, Wang L, Liu JF, Wei Y, Li Y (2007) Bifunctional Au-Fe₃O₄ Nanoparticles for Protein Separation. *ACS Nano* 1: 293 – 298.
- [10] Meledandri CJ, Stolarczyk JK, Brougham DF (2011) Hierarchical Gold-Decorated Magnetic Nanoparticle Clusters with Controlled Size. *ACS Nano* 5: 1747 – 1755.
- [11] Liu Y, Han T, Chen C, Bao N, Yu CM, Gu HY (2011) A novel platform of hemoglobin on core-shell structurally Fe₃O₄@Au nanoparticles and its direct electrochemistry. *Electrochim. Acta* 56: 3238–3247.
- [12] Lyon JL, Fleming DA, Stone M-B, Schiffer P, Williams ME (2004) Synthesis of Fe Oxide Core/Au Shell Nanoparticles by Iterative Hydroxylamine Seeding. *Nano Lett.* 4: 719 – 723.
- [13] Kim J, Park S, Lee JE, Jin SM, Lee IS, Yang I, Kim JS, Kim SK, Cho MH, Hyeon T (2006) Designed Fabrication of Multifunctional Magnetic Gold Nanoshells and Their Application to Magnetic Resonance Imaging and Photothermal Therapy. *Angew. Chem. Int. Ed.* 45: 7754 – 7758.
- [14] Caruntu D, Cushing BL, Carunt G, O'Connor CJ (2005) Attachment of Gold Nanograins onto Colloidal Magnetite Nanocrystals. *Chem. Mater.* 17: 3398 – 3402.
- [15] Ojea-Jimenez I, Lorenzo J, Rebled JM, Sendra J, Arbiol J, Puentes V (2012) Synthesis of Co-organosilane-Au nanocomposites via a controlled iterphasic reduction. *Chem. Mater.* 24: 4019 – 4027.
- [16] Chen M, Yamamuro S, Farell D, Majetich SA (2003) Gold coated iron nanoparticles for biomedical applications. *J. Appl. Phys.* 93: 7551 – 7553.
- [17] Xu Z, Hou Y, Sun, S (2007) Magnetic Core/Shell Fe₃O₄/Au and Fe₃O₄/Au/Ag Nanoparticles with Tunable Plasmonic Properties. *J. Am. Chem. Soc.* 129: 8698–8699.
- [18] Ban Z, Barnakov YA, Li F, Golub VO, O'Connor CJ (2005) The synthesis of core-shell iron@gold nanoparticles and their characterization. *J. Mater. Chem.* 15: 4660 – 4662.
- [19] Spasova M, Salgueirino-Maceira V, Schlachter A, Hilgendorff M, Giersig M, Liz-Marzan LM, Farle M (2005) Magnetic and optical tunable microspheres with a magnetite/gold nanoparticle shell, *J. Mater. Chem.* 15: 2095 – 2098.
- [20] Wu W, He Q, Chen H, Tang J, Nie L (2007) Sonochemical synthesis, structure and magnetic properties of air-stable Fe₃O₄/Au nanoparticles. *Nanotechnology* 18: 145609.
- [21] Zhang J, Post M, Veres T, Jakubek ZJ J, Guan J, Wang D, Normandin F, Deslandes Y, Simard B (2006) Laser-Assisted Synthesis of Superparamagnetic Fe@Au Core-Shell Nanoparticles. *J. Phys. Chem. B* 110: 7122 – 7128.
- [22] Yu H, Chen M, Rice PM, Wang SX, White RL, Sun S (2005) Dumbbell-like bifunctional Au-Fe₃O₄ nanoparticles. *Nano Lett.* 5: 379 – 382
- [23] Wu A, Ou P, Zeng L (2010) Biomedical applications of magnetic nanoparticles, *NANO* 5: 245 – 270.
- [24] Fan Z, Shelton M, Singh AK, Senapati D, Khan SA, Ray PC (2012) Multifunctional Plasmonic Shell-Magnetic Core Nanoparticles for Targeted Diagnostics, Isolation, and Photothermal Destruction of Tumor Cells. *ACS Nano* 6: 1065 – 1073.
- [25] Yu Q, Shi M, Cheng W, Wang M, Chen H (2008) Fe₃O₄@Au/polyaniline multifunctional nanocomposites: their preparation and optical, electrical and magnetic properties. *Nanotechnology* 19: 265702.
- [26] Cui Y, Wang Y, Hui W, Zhang Z, Xin X, Chen C (2005) The synthesis of gold mag nano-particles and their application for antibody immobilization, *Biomed. Microdev.* 7: 153 –156.
- [27] Lin J, Zhou W, Kumbhar A, Wiemann J, Fang J, Carpenter EE, O'Connor CJ (2001) Gold-Coated Iron (Fe@Au) Nanoparticles: Synthesis, Characterization, and Magnetic Field-Induced Self-Assembly. *J. Solid State Chem.* 159: 26 – 31.
- [28] Tamer U, Gundogdu Y, Boyaci IH, Pekmez K (2010) Synthesis of magnetic core-shell Fe₃O₄-Au nanoparticle for biomolecule immobilization and detection. *J. Nanopart. Res.* 12: 1187 – 1196.
- [29] Mandal S, Krishnan KM (2007) Co_{core}Au_{shell} nanoparticles: evolution of magnetic properties in the displacement reaction. *J. Mater. Chem.* 17: 372 – 376.
- [30] Jagminas A, Kurtinaitienė M, Mažeika K (2013) Synthesis of cobalt ferrite nanoparticles by complex-assisted co-precipitation and hydrothermal approaches. *Chemija* 24(2): 103-110.
- [31] Roca AG, Costo R, Rebollo AF, Veintemillas-Verdaguer, S Tartaj P, Gonzalez-Carreño T, Morales MP, Serna CJ (2009) Progress in the preparation of magnetic nanoparticles for applications in biomedicine. *J. Phys. D: Appl. Phys.* 42: 224002.
- [32] Taleb A, Petit C, Pileni MP (1997) Synthesis of Highly Monodisperse Silver Nanoparticles from AOT Reverse Micelles: A Way to 2D and 3D Self-Organization *Chem. Mater.* 9: 950 – 959.

- [33] Xie YW, Ye RQ, Liu H (2006) Synthesis of silver nanoparticles in reverse micelles stabilized by natural biosurfactant. *Colloids Surf. A* 279: 175 – 178.
- [34] Wang L, Wang L, Luo J, Fan Q, Suzuki M, Suzuki IS, Engelhard MH, Lin Y, Kim N, Wang JQ, Zhong C-J (2005) Monodispersed core-shell $\text{Fe}_3\text{O}_4@Au$ nanoparticles. *J. Phys. Chem. B* 109: 21593 – 21601.